RSC Advances

ROYAL SOCIETY OF CHEMISTRY

www.rsc.org/advances

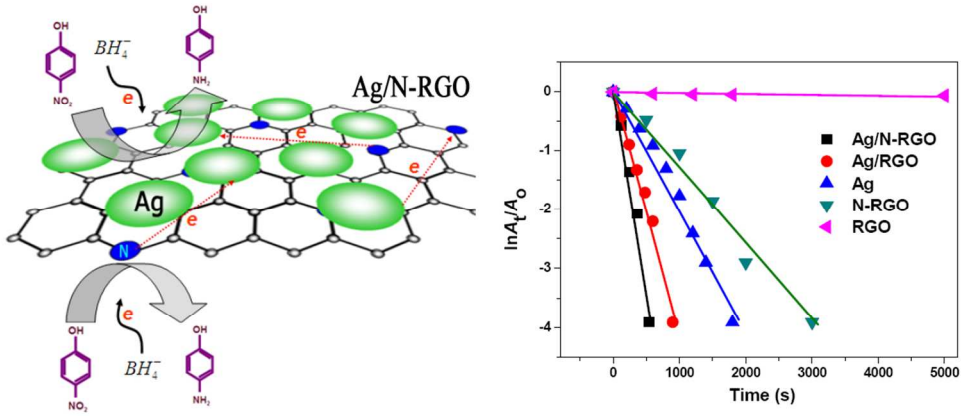

419x177mm (72 x 72 DPI)

Ag nanoparticles supported on N-doped graphene hybrids for catalytic reduction of 4-nitrophenol

Ye Tian[1], Yan-yan Cao[2], Fu Pang[3], Gui-qiang Chen[2], Xiao Zhang[2,*]

[1] *Department of Physics, College of Science, Hebei North University, Zhangjiakou, Hebei 075000, China*

[2] *Colleges of Information Science and Engineering, Hebei North University, Zhangjiakou, Hebei 075000, China*

[3] *Department of Electrical Engineering, Zhangjiakou Vocational College of Technology, Zhangjiakou, Hebei 075000, China*

Abstract

Ag nanoparticles (NPs) supported on N-doped reduced graphene oxide (Ag/N-RGO) hybrids were prepared by a combined solvothermal approach and microwave-polyol method. Compared to Ag NPs grown on undoped reduced graphene oxide (Ag/RGO), Ag/N-RGO exhibited better NPs dispersion, smaller particle size, and stronger NPs-graphene interactions. The catalytic ability of Ag/N-RGO was evaluated for the reduction of 4-nitrophenol (4-NP) to 4-aminophenol (4-AP) with $NaBH_4$, revealing that Ag/N-RGO showed a higher catalytic ability than Ag NPs or N-RGO alone, and Ag/RGO, which was due *possibly* to the synergetic effects between Ag NPs and N-RGO. Furthermore, the durability of Ag/N-RGO was much better than that of Ag/RGO. These results indicates that Ag/N-RGO has a great potential for application in catalytic reduction of 4-NP.

Keywords: N-doped graphene; Graphene hybrids; Solvothermal synthesis; Catalytic reduction.

*Corresponding author. E-mail address: Zhangxiao83690@163.com (X. Zhang)

1 Introduction

4-Nitrophenol (4-NP) and related compounds are common organic pollutants that often exist in industrial and agricultural wastewaters, and it is necessary to remove them from the polluted waters to meet increasingly stringent environmental quality standards[1]. Among all the 4-NP removal methods, the catalytic reduction of 4-NP to 4-aminophenol (4-AP) with $NaBH_4$ is the most extensively adopted method because of its high efficiency, cost-effective and simple operation[2]. Additionally, as the reduction product, 4-AP is an important intermediate for the manufacture of pharmaceuticals, dyes, explosives, papers, polymers, corrosion inhibitor, and anticorrosion-lubricant[3].

The catalytic reduction of 4-NP to 4-AP by noble metallic nanoparticles (NPs), such as Au, Ag, Pt, Pd, etc, has received increasing attention due to their high catalytic performance as heterogeneous catalysts in numerous liquid-phase catalytic processes[3-5]. Among these noble metallic NPs, Ag is particularly attractive because of its environmental friendship and low cost compared to other noble metals such as Au, Pt, and Pd[6]. However, pure Ag NPs very easily aggregate to significantly minimize their surface area, leading to the reduction in catalytic activity and difficulty in catalyst recycling. To overcome the aggregation problem, many efforts have been devoted to developing hybrid catalysts by immobilizing metal NPs on/into various support materials, such as carbon (active carbon[7], carbon nanotubes[8], and carbon nanofibers[9]), silica[10], zeolites[11], and conducting polymers[12], which is considered as an effective strategy in protecting these metal NPs against agglomeration and improving

their catalytic activity and durability. Because of its unique structure and excellent properties, graphene has attracted extensive attention to be an ideal support material for hybrid catalysts due to its high specific surface area, ultrathin thickness, chemical stability, and remarkable electrical properties[13-15]. Extensive studies have been carried out on graphene-NPs hybrids, which show great potential for diverse applications in catalysis, sensors, batteries, supercapacitors, and hydrogen storage[16-18]. It has been demonstrated that metal NPs can be strongly coupled into a graphene support to improve their catalytic activity and stability for 4-NP reduction[19-21].

Doped graphene, namely, the engineering of pristine graphene by incorporation of heteroatoms, such as N, B, P, and S, into the graphitic structure, is an effective way to modify the electron-donor properties of graphene and consequently to further enhance its catalytic activity[22]. Currently, N-doping graphene (N-G) has received most interests because of its large ratio of surface active groups to volume, high electrical conductivity and abundant chemically active sites[22]. More importantly, N-dopants can serve as active sites for anchoring metal NPs, strengthening metal-graphene interactions and resulting in enhanced stability[23]. It has been reported that Pt NPs supported on N-G exhibited significantly enhanced catalytic activity and durability compared to undoped counterparts toward oxygen reduction reaction[24]. Therefore, it is also expected that metal NPs supported on N-G hybrids would potentially provide an excellent catalytic activity for the reduction of 4-NP. However, no attention so far has been paid to employ Ag/N-G as a catalyst for the reduction of 4-NP.

In this study, we reported the development of Ag NPs supported on N-doped reduced graphene oxide (Ag/N-RGO) hybrids, and evaluated their catalytic performance for catalytic reduction of 4-NP. Ag/N-RGO was prepared through a two-step procedure (**Scheme 1**), in which N-RGO was first obtained by the solvothermal reaction of graphene oxide (GO) and ammonia, then the Ag NPs was deposited onto N-RGO sheets by a modified microwave-polyol method. The morphology, structure, and catalytic activity of both undoped Ag/RGO and Ag/N-RGO catalysts were studied in detail. It was shown that Ag/N-RGO exhibited much higher catalytic activity and better durability than Ag/RGO for the catalytic reduction of 4-NP to 4-AP with $NaBH_4$.

2 Experimental

2.1. Synthesis of N-RGO

All the chemicals were purchased from Tianjin Chemical Reagent Co., China, and used without further purification. GO was prepared by chemical oxidation and exfoliation of natural graphite following a modified Hummer's method[25]. N-RGO was synthesized by a one-pot solvothermal route using ammonia as the N-dopant[14]. In brief, 2 g GO powder was dispersed in 500 *mL* water by sonication for 1 h to form a stable GO colloid, followed by the addition of 200 *mL* ammonia with sonication for 10 min. The resulting solution was sealed in a Teflon-lined autoclave and treated at 190 ^{o}C for 10 h. After cooling to room temperature naturally, the solid product was obtained by centrifugation, washed with distilled water and freeze drying. The undoped reduced graphene oxide (RGO) was also obtained through the same

procedure as N-RGO without adding ammonia in the first step.

2.2. Synthesis of Ag/N-RGO

Ag/N-RGO hybrids were synthesized by a modified microwave-polyol method which involved the chemical reduction of Ag ions in ethylene glycol (EG) solution with $NaBH_4$ as reducing agent under microwave treatment[26]. In a typical synthesis, 1 g N-RGO was dispersed in 200 *mL* EG under sonication for 30 min. Then, 0.2 g $AgNO_3$ and 20 mg $NaBH_4$ were co-added into the above suspension. After sonication for 1 h, the suspension was treated at 150^{o}C for 5 min in a microwave oven (800W maximum power input). After cooling to room temperature naturally, the solid product was obtained by centrifugation, washed with distilled water and freeze drying. Ag/RGO was prepared through the same procedure as Ag/N-RGO by replacing N-RGO with RGO in the first step. Ag NPs were also prepared through the same procedure as Ag/N-RGO without adding GO in the first step.

2.3. Catalysis study

To perform the catalysis test, the reduction of 4-NP to 4-AP by excess $NaBH_4$ at room temperature was chosen as a model reaction[27]. Briefly, 0.2 mM 4-NP solution and 0.2 M $NaBH_4$ solution were freshly prepared. Then, 1.5 *mL* aqueous 4-NP solution and 2.0 *mL* $NaBH_4$ solution was mixed in a quartz cuvette, and a color change from light yellow to deep yellow can be observed. After that, 0.1 mL Ag/N-RGO (10 mg/mL, *54.2 wt.% Ag loading in the hybrid (TGA)*) suspension was added to start the reaction with continuous stirring. The reaction progress was monitored by a UV-vis spectroscopy (UV5800 spectrophotometer) at a regular time

interval (100s) until the deep yellow solution became colorless. *The catalyst precipitations were not observed throughout the reaction and UV-vis measurement process.* For comparison, the catalytic activities of Ag/RGO *(56.3 wt.% Ag loading in the hybrid)*, Ag NPs, N-RGO and RGO with the same amount (1 mg) were also tested respectively following the same procedures. For the recycling experiment, the catalysts were recovered by centrifugation, washed several times with deionized water and ethanol, and then reused.

2.4. Characterizations

Transmission electron microscopy (TEM, JEM-2100) was used for morphology observations. X-Ray diffraction (XRD) pattern was recorded on a Bruker D8 Avance diffractometer using Cu Kα radiation. X-ray photoelectron spectroscopy (XPS) measurement was conducted on a PHI 5000C ESCA system. Raman spectra were recorded on a Raman spectroscope (Alpha 300R, WITEC) using a 633 nm laser source. Surface area measurement was carried out using a Brunauer−Emmett−Teller (BET) method. Thermogravimetric analysis (TGA) was conducted on a Q50 TGA instrument at a heating rate of 10 ^{o}C/min under air atmosphere. The electrical conductivity of the samples was measured by a four probe method.

3 Results and discussion

3.1. Preparation and characterization of Ag/N-RGO

The synthesis mechanism of the Ag/N-RGO hybrids is illustrated in **Scheme 1**. First, GO colloid mixed with ammonia under solvothermal treatment leads to the reduction of GO and the simultaneous incorporation of N species into the graphene

lattice to form N-RGO. After adding $AgNO_3$, the residue oxygenated functional groups along with N-doping species present on N-RGO sheets provide anchoring sites for binding Ag^+ ions to form a Ag^+/N-RGO complex. Subsequently, the introduction of $NaHB_4$ under microwave treatment induces *in situ* nucleation and growth of Ag nanocrystals on the N-RGO surface, resulting in the Ag/N-RGO hybrids. In this process, N-doping species are expected to increase the metal-support interactions and thus to facilitate the growth of smaller-sized Ag NPs and also their uniform dispersion.

XRD measurements were employed to investigate the phase of the as-synthesized Ag/RGO and Ag/N-RGO, as shown **Fig. 1**. Noticeably, the peaks at 2θ of 38.5 °, 44.1 °, 64.2 °, and 77.1° are assigned to the (1 1 1), (2 0 0), (2 2 0), and (3 1 1) planes of the face centered cubic Ag (JCPDS No. 04-0783), respectively, indicating that the NPs in both Ag/N-RGO and Ag/RGO are metallic Ag NPs. The average particle size can be readily calculated by a Scherrer equation[28]. From the full-width half-maximum of the (1 1 1) peak, the average Ag particle sizes are 13.2 and 21.3 nm for Ag/N-RGO and Ag/RGO, respectively. Additionally, the weak and broaden graphene (002) peaks appearing at ~24.5 ° suggest the high-degree exfoliation of the graphene sheets in both Ag/N-RGO and Ag/RGO due to the insertion of Ag NPs. The XRD results demonstrate that metallic Ag NPs could be successfully incorporated with either N-RGO or RGO.

Fig. 2 shows the TEM images of RGO, N-RGO, Ag/N-RGO and Ag/RGO. It is clear that the morphologies of the RGO (**Fig. 2(a)**) and N-RGO (**Fig. 2(b)**) are similar,

showing characteristically folded and rippled structures, which are also observed in their SEM images (**Fig. S1, Supporting Information**). The selected area electron diffraction (SAED) patterns are also shown. The hexagonal diffraction spots (**Fig. 2(a) inset**) indicate that RGO still keeps a well-ordered crystalline structure. However, N-RGO (**Fig. 2(b) inset**) reveals a ring-like diffraction pattern with symmetric hexagonal dispersed spots, suggesting the structure distortion after N-doping[29]. As shown in **Figs. 2(c, d)**, Ag/N-RGO exhibits a better dispersion of Ag NPs than Ag/RGO, in which Ag NPs deposited on N-RGO shows a smaller average particle size with a narrower size distribution (10 nm, 5–15 nm, **Fig. 2(d) inset**) than those on undoped RGO (18 nm, 5–30 nm, **Fig. 2(c) inset**). These observations suggest that the doping of graphene with N species can well suppress the particle growth and aid the formation of small-sized AgNPs, owing to the strong coordination of N species with AgNPs in reducing particle size[14]. The same phenomenon was also found in other N-G based hybrids[14, 30].

Fig. 3 shows the TGA curves of Ag/RGO and Ag/N-RGO under air flow. The weight loss at the temperature below 100 °C is attributed to the evaporation of moisture. For Ag/RGO, the significant weight loss in the range of 300~500 °C is caused by the combustion of the carbon skeleton of graphene. The weight change of Ag/N-RGO follows a similar trend but shows a significant weight loss shifting to the upper temperature range of 350~550 °C, *which is because N-RGO itself is more stable than RGO (**Fig. S2, Supporting Information**).* In addition, the whole weight loss of Ag/N-RGO is slightly lower than that of Ag/RGO, especially in the range of

500~700 °C, which is considered to be caused by the smaller Ag NPs size of Ag/N-RGO (**Fig. 2(d)**), since the smaller NPs will be oxidized at a faster rate and thus result in a more weight increase. Furthermore, the weight percentage of graphene in the hybrids can be estimated by determining the weight loss in the range of 300~550 °C, which are 56.3 wt.% for Ag/RGO and 54.2 wt.% for Ag/N-RGO.

Chemical compositions of Ag/RGO and Ag/N-RGO were analyzed by XPS, as shown in **Fig. 4**. **Fig. 4(a)** shows the XPS survey spectra of Ag/RGO and Ag/N-RGO, and the peaks at binding energies of 284.5 eV, 370.0 eV 400.0 eV, and 532.5 eV can be assigned to C 1s, Ag 3d, N 1s, and O 1s, respectively. **Table 1** lists the elements analysis and functional groups percentage of Ag/RGO and Ag/N-RGO obtained from the XPS results. The XPS analysis reveals 4.38 at.% N in the Ag/N-RGO, but not in the Ag/RGO sample, indicating that ammonia is *an* effective N-dopant to prepare N-RGO, in accordance with other reports[31, 32]. In addition, the lower level of O element in Ag/N-RGO (11.67 at.%) than that in Ag/RGO (15.21 at.%) indicates that the ammonia is not only a nitrogen source but also is very effective in the deoxidation of oxygen-containing functional groups in GO during the solvothermal process. The C1s spectrum of Ag/N-RGO (**Fig. 4(b)**) can be deconvoluted into five carbon functional groups: 77.12% C-C (284.5 eV), 9.32% C-N (285.9 eV), 6.75% C-O (286.5 eV), 4.56% C=O (287.9 eV) and 2.25% O-C=O (289.1 eV)[30], whereas C-N functional groups can not *be* found in the C1s spectrum of Ag/RGO (**Fig. S3, Supporting Information**). The deconvolution of the N1s spectrum of Ag/N-RGO (**Fig. 4(c)**) shows three kinds of N species: 46.91% pyridine-N (398.8 eV), 21.56%

pyrrole-N (400.3 eV), and 31.53% graphitic-N (401.4 eV)[31], suggesting the successful N-doping and the pyridine N is the major N component in Ag/N-RGO. It has been demonstrated that the pyridinic-N plays a major role in enhancing the binding between Pt NPs and N-doped graphene[24]. Hence the high content of pyridinic-N in Ag/N-RGO contributes a strong adhesion of Ag NPs on N-RGO. **Fig. 4(d)** shows the Ag 3d XPS spectra of Ag/RGO and Ag/N-RGO. The Ag $3d_{5/2}$ and Ag $3d_{3/2}$ peaks are at 367.2 and 372.9 eV for Ag/RGO, and at 367.8 and 373.6 eV for Ag/N-RGO, respectively, indicating a positive shift Ag 3d spectra for Ag/N-RGO in comparison to Ag/RGO. The positive shift of Ag 3d XPS core levels may arise from *the smaller particle size of Ag NPs on N-RGO*[33, 34], or the improved electrons transfer from Ag NPs to N-RGO caused by the enhanced Ag-N-RGO interactions[35].

Raman spectroscopy was used to characterize the carbon structures of Ag/RGO and Ag/N-RGO, as shown in **Fig. 5**. In the Raman spectra, the G band corresponds to sp^2-hybridized carbons in a hexagonal lattice, the D band is related to the vibrations of sp^3-hybridized of graphene with structural defects and disorders[36]. In general, the D/G intensity ratio (ID/IG) reflects the defect density in carbon materials, and it is 1.15 and 1.28 for Ag/RGO and Ag/N-RGO, respectively. The increased ID/IG in Ag/N-RGO is due possible to the broken hexagonal lattice structure and increased defects by N-doping. Furthermore, the G band of Ag/N-RGO down-shifts to 1569 cm^{-1} compared to that of Ag/ RGO at 1577 cm^{-1}, which is also related to N-doping, since the G band is sensitive to the chemical doping state and N-doping can lead to the modified carbon structure and therefore the downshift of the G band[29].

3.2. Catalytic properties of Ag/N-RGO

The catalytic performance of Ag/N-RGO was investigated by reduction reaction of 4-NP into 4-AP with a large excess of $NaBH_4$. For comparison, Ag/RGO, Ag NPs, N-RGO and RGO were also investigated. **Fig. 6 (a)** shows the time dependent catalytic process monitored by UV−vis spectroscopy using Ag/N-RGO as the catalyst. As seen, the addition of Ag/N-RGO to 4-NP solution leads to the successive decrease of the peak intensity of 4-NP at 400 nm accompanied by the increase of the peak intensity of 4-AP at 300 nm, indicating the decay of 4-NP and the formation of 4-AP instead. After 400 s, the peak of the 4-NP is no longer observed, implying the complete catalytic reduction of 4-NP to 4AP. In contrast, as shown in **Fig. 6 (b)**, the absorbance peak at 400 nm disappears completely after a longer time of 900s using Ag/RGO as catalyst, suggesting the weaker catalytic activity of Ag/RGO than Ag/N-RGO. However, a much longer reaction time is required to achieve the full reduction of 4-NP using Ag NPs (1800s) or N-RGO (3000s) alone as catalyst, while RGO alone is found to be inactive (**Fig. S4, Supporting Information**). Because of the much higher concentration of $NaBH_4$ compared to that of 4-NP, the pseudo-first-order kinetics could be applied in order to quantitatively determine the catalytic activity of above catalysts[37]. The plots of ln (A_t/A_0) vs. the reaction time (t) for all the catalysts (Ag/N-RGO, Ag/RGO, Ag NPs, N-RGO, and RGO) are shown in (**Fig. 6 (c)**), where A_t and A_0 are the time-dependent and initial (t=0) absorbance of the 400 nm peak, respectively. The reaction rate constants (k) can be calculated from the slope of the linear fit of ln (A_t/A_0) vs. t, which is summarized in **Table 2**. It is obvious

that, among all the catalysts, Ag/N-RGO exhibits the highest rate constant of 7.4×10^{-3}/s, which is 2.1 times that of Ag/N-RGO (3.6×10^{-3}/s), 3.5 times that of Ag NPs (2.1×10^{-3}/s), indicating the excellent catalytic activity of Ag/N-RGO. The above results clearly indicate that although Ag NPs or RGO alone has a low catalytic activity, their hybrid exhibits a significantly enhanced catalytic activity that is further improved by N-doping of RGO (N-RGO).

Although the underlying mechanisms for the excellent catalytic activity of the Ag/N-RGO hybrids remain unclear, we tentatively propose the following mechanisms according to the experimental results, as illustrated in **Scheme 2**. It is well known that the reduction of 4-NP to 4-AP with $NaBH_4$ does not proceed without catalysts due to the large kinetic barrier between the mutually repelling negative ions 4-NP and BH_4^- [38]. Once the catalysts, such as Ag NPs are added, Ag NPs can act as electronic relays to effectively transfer electrons donated by BH_4^- to the nitro groups of 4-NP, which decreases the kinetic barrier and increases the reduction rate of 4-NP to 4-AP [39]. Thus the rate of catalytic reaction depends on two factors, namely, adsorption of 4-NP to the catalyst surface, and electron transfer mediated by the catalyst surface from BH_4^- to 4-NP. **(i)** Generally speaking, the adsorption ability is relative to the BET specific surface area of the materials. The Ag NPs loaded on the N-RGO show a smaller particle size compared to their undoped counterparts (**Figs. 2(c, d)**), and smaller particle size leads to a larger specific surface area (165.8 m^2/g for Ag/N-RGO, 148.2 m^2/g for Ag/RGO, **Table S1, Supporting Information)**), which therefore provides more active sites for the catalytic reaction. **(ii)** N-doping could improve the chemical

reactivity and electronic conductivity of the graphene by changing their electronic structures. For instance, the pyridinic-N can provide a pair of electrons for conjugation with the π-conjugated rings which can introduce electron donor properties that are responsible for the increased electrical conductivity[40]. In order to examine the electrical conductivity, the RGO and N-RGO films were prepared with the same thickness by a vacuum filtration method[41], and their electrical conductivity was measured (**Fig. S5 and Table S2, Supporting Information**). The electrical conductivity of RGO is determined as 4.25 S/m, which is increased substantially to 33.68 S/m for N-RGO. Hence, highly conductive N-RGO enhances the electron-donor characteristics of the supporting Ag catalysts and induces a further improvement of catalytic performance. **(iii)** It has been confirmed that even the N-RGO shows a much enhanced catalytic activity relative to RGO (**Fig. S3, Supporting Information**). A recent publication gave the insights for the reduction of 4-NP using N-RGO alone as catalyst both experimentally and theoretically, revealing that all kinds of N-doping species (pyridine-N, pyrrole-N, graphitic-N) are favorable for 4-NP adsorption and the 4-NP ions tend to interact with these N-doping species *via* the O atom of the hydroxyl group owing to its weakened conjugation as well as higher positive charge density[42]. Therefore the N-doping species would be exposed and act as secondary active sites to drive the catalytic reaction (**Scheme 2**). Therefore, all the factors of enhanced adsorption ability, improved conductivity, and additional active sites introduced by N-RGO itself make Ag/N-RGO hybrids exhibit enhanced catalytic activity. However, which factor plays a major role is still not clear and needs

further investigation.

Finally, the durability of our Ag/N-RGO catalyst in long-term operation was evaluated under the same reaction conditions as that of the first cycle, as shown in **Fig. 7.** As seen, Ag/N-RGO was reused for ten cycles with a stable conversion efficiency of more than 92.3%. However, the conversion efficiency of Ag/RGO is reduced to about 77.6% after ten cycles, suggesting that Ag/N-RGO shows a superior durability over the Ag/RGO catalyst. As confirmed previously (**Fig. 3, Fig. 4(d)**), N-doping contributes to the effective immobilization of Ag NPs due to strong coordination interactions between Ag NPs and N-RGO. The strong interactions of Ag NPs to N-RGO can effectively prevent the NPs from agglomerations and exfoliation from the supports during the cycling tests and thus make Ag/N-RGO have higher catalytic durability, whereas the interactions between Ag NPs and RGO in Ag/RGO are not strong enough to maintain the catalyst durability ***(Fig. S6, Supporting Information)***. Therefore, the outstanding features of high activity and strong durability indicate that Ag/N-RGO is a potential catalyst for application in 4-NP reduction.

4 Conclusions

In summary, through the combination of solvothermal approach and microwave-polyol method, we have successfully fabricated Ag/N-RGO hybrids. Compared to the undoped Ag/RGO, Ag/N-RGO showed better dispersion, smaller average particle size, and stronger NPs-graphene interactions. Furthermore, the resulting Ag/N-RGO hybrids exhibited a higher catalytic activity for the reduction of 4-NP to 4-AP with $NaBH_4$, than Ag NPs or N-RGO alone, and Ag/RGO. A significant enhancement in

the catalytic performance of Ag/N-RGO originated from the synergetic effects between supported Ag NPs and N-RGO sheets, including enhanced adsorption ability, improved conductivity, and additional active sites introduced by N-RGO itself. Moreover, Ag/N-RGO offered a great durability over the Ag/RGO catalyst, thereby displaying their potential application in catalytic reduction of 4-NP.

Acknowledgements

This work was supported by the Science and Technology Department of Hebei Province Project (No.13210336), financially supported by National Ministry of Science and Technology Project (No.2012BAJ18B08-6) and Zhangjiakou Science and Technology Bureau Project (No.13110038I-11).

Reference

1. D. Chen and A. K. Ray, *Water Res.*, 1998, **32**, 3223-3234.
2. N. Pradhan, A. Pal and T. Pal, *Colloid. Surface. A*, 2002, **196**, 247-257.
3. S. Saha, A. Pal, S. Kundu, S. Basu and T. Pal, *Langmuir*, 2009, **26**, 2885-2893.
4. A. Gangula, R. Podila, L. Karanam, C. Janardhana and A. M. Rao, *Langmuir*, 2011, **27**, 15268-15274.
5. S. Panigrahi, S. Basu, S. Praharaj, S. Pande, S. Jana, A. Pal, S. K. Ghosh and T. Pal, *J. Phys. Chem. C.*, 2007, **111**, 4596-4605.
6. G.-W. Yang, G.-Y. Gao, C. Wang, C.-L. Xu and H.-L. Li, *Carbon*, 2008, **46**, 747-752.
7. J. Zazo, J. Casas, A. Mohedano and J. Rodriguez, *Appl. Catal. B: Environ.*, 2006, **65**, 261-268.
8. V. Georgakilas, D. Gournis, V. Tzitzios, L. Pasquato, D. M. Guldi and M. Prato, *J. Mater. Chem.*, 2007, **17**, 2679-2694.
9. P. Zhang, C. Shao, Z. Zhang, M. Zhang, J. Mu, Z. Guo and Y. Liu, *Nanoscale*, 2011, **3**, 3357-3363.
10. T. Zhang and M. D. Amiridis, *Appl. Catal. A: Gen*, 1998, **167**, 161-172.
11. J.-S. Chang, S.-E. Park and H. Chon, *Appl. Catal. A: Gen*, 1996, **145**, 111-124.
12. S. Bouazza, V. Alonzo and D. Hauchard, *Synthetic Met.*, 2009, **159**, 1612-1619.
13. Y. Li, L. Tang and J. Li, *Electrochem. Commun.*, 2009, **11**, 846-849.
14. Y. Liang, Y. Li, H. Wang, J. Zhou, J. Wang, T. Regier and H. Dai, *Nature Mater.*, 2011, **10**, 780-786.
15. A. A. Balandin, *Nature Mater.*, 2011, **10**, 569-581.
16. C. Xu, X. Wang and J. Zhu, *J. Phys. Chem. C.*, 2008, **112**, 19841-19845.
17. P. V. Kamat, *J. Phys. Chem. Lett.*, 2009, **1**, 520-527.

18. X. Zhou, X. Huang, X. Qi, S. Wu, C. Xue, F. Y. Boey, Q. Yan, P. Chen and H. Zhang, *J. Phys. Chem. C.*, 2009, **113**, 10842-10846.
19. J. Li, C.-y. Liu and Y. Liu, *J. Mater. Chem.*, 2012, **22**, 8426-8430.
20. Y. Choi, H. S. Bae, E. Seo, S. Jang, K. H. Park and B.-S. Kim, *J. Mater. Chem.*, 2011, **21**, 15431-15436.
21. Y. Zhang, S. Liu, W. Lu, L. Wang, J. Tian and X. Sun, *Catal. Sci. Technol.*, 2011, **1**, 1142-1144.
22. L. Panchakarla, K. Subrahmanyam, S. Saha, A. Govindaraj, H. Krishnamurthy, U. Waghmare and C. Rao, *Adv. Mater.*, 2009, **21**, 4726-4730.
23. L.-S. Zhang, X.-Q. Liang, W.-G. Song and Z.-Y. Wu, *Phys. Chem. Chem. Phys.*, 2010, **12**, 12055-12059.
24. D. He, Y. Jiang, H. Lv, M. Pan and S. Mu, *Appl. Catal. B: Environ.*, 2013, **132**, 379-388.
25. D. Li, M. B. Müller, S. Gilje, R. B. Kaner and G. G. Wallace, *Nature Nanotechnol.*, 2008, **3**, 101-105.
26. S. Komarneni, D. Li, B. Newalkar, H. Katsuki and A. S. Bhalla, *Langmuir*, 2002, **18**, 5959-5962.
27. K. Hayakawa, T. Yoshimura and K. Esumi, *Langmuir*, 2003, **19**, 5517-5521.
28. A. Patterson, *Phys. Rev.*, 1939, **56**, 978.
29. H. Wang, T. Maiyalagan and X. Wang, *Acs Catal.*, 2012, **2**, 781-794.
30. B. Xiong, Y. Zhou, Y. Zhao, J. Wang, X. Chen, R. O'Hayre and Z. Shao, *Carbon*, 2013, **52**, 181-192.
31. L. Qu, Y. Liu, J.-B. Baek and L. Dai, *ACS nano*, 2010, **4**, 1321-1326.
32. Y. Shao, S. Zhang, M. H. Engelhard, G. Li, G. Shao, Y. Wang, J. Liu, I. A. Aksay and Y. Lin, *J. Mater. Chem.*, 2010, **20**, 7491-7496.
33. *L. Chen, A. Yelon and E. Sacher, J. Phys. Chem. C., 2011, **115**, 12972-12980.*
34. *L. Chen, A. Yelon and E. Sacher, J. Phys. Chem. C., 2011, **115**, 7896-7905.*
35. Q. Zhang, C. Tian, A. Wu, T. Tan, L. Sun, L. Wang and H. Fu, *J. Mater. Chem.*, 2012, **22**, 11778-11784.
36. A. Ferrari, J. Meyer, V. Scardaci, C. Casiraghi, M. Lazzeri, F. Mauri, S. Piscanec, D. Jiang, K. Novoselov and S. Roth, *Phys. Rev. Lett.*, 2006, **97**, 187401.
37. S. Chakrabarti and B. K. Dutta, *J. Hazard. Mater.*, 2004, **112**, 269-278.
38. Z. Zhang, C. Shao, Y. Sun, J. Mu, M. Zhang, P. Zhang, Z. Guo, P. Liang, C. Wang and Y. Liu, *J. Mater. Chem.*, 2012, **22**, 1387-1395.
39. K. Kuroda, T. Ishida and M. Haruta, *J. Mol. Catal. A: Chem.*, 2009, **298**, 7-11.
40. D. Deng, X. Pan, L. Yu, Y. Cui, Y. Jiang, J. Qi, W.-X. Li, Q. Fu, X. Ma and Q. Xue, *Chem. Mater.*, 2011, **23**, 1188-1193.
41. D. A. Dikin, S. Stankovich, E. J. Zimney, R. D. Piner, G. H. Dommett, G. Evmenenko, S. T. Nguyen and R. S. Ruoff, *Nature*, 2007, **448**, 457-460.
42. X.-K. Kong, Z.-Y. Sun, M. Chen and Q.-W. Chen, *Energ. Environ. Sci.*, 2013, **6**, 3260-3266.

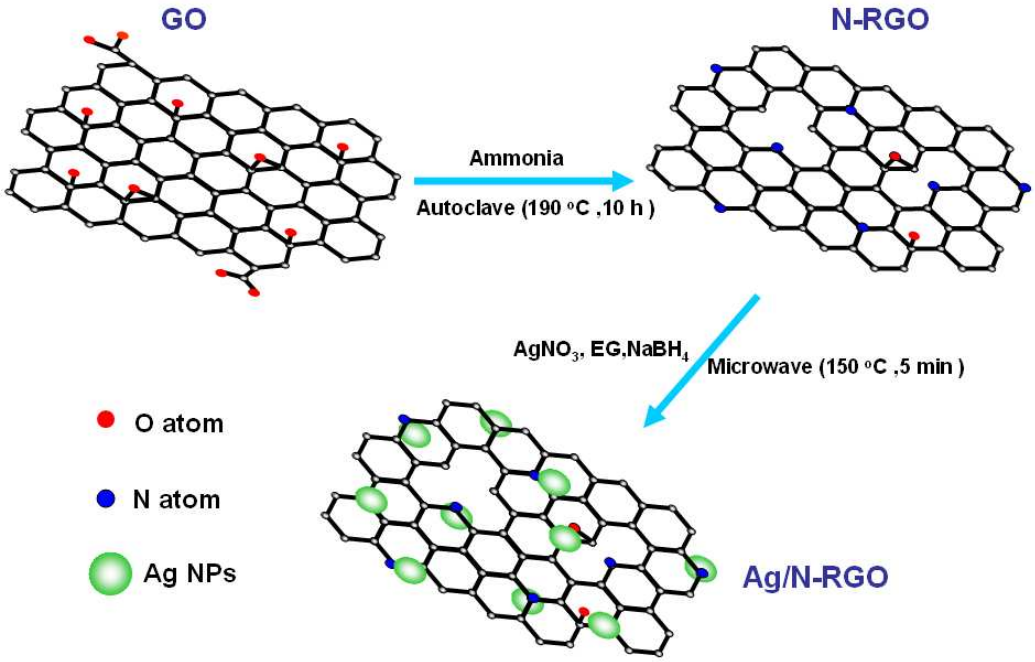

Scheme 1. Schematic diagram of the synthesis procedure of Ag/N-RGO

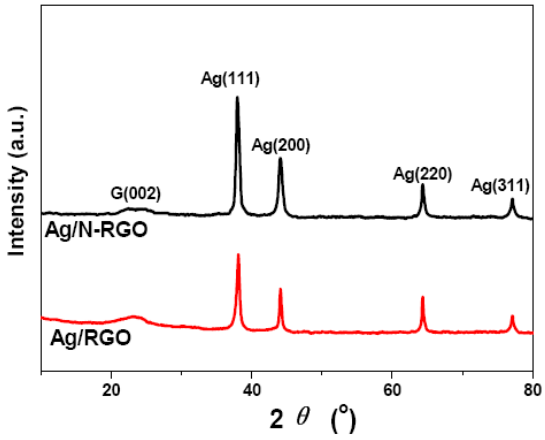

Fig. 1. XRD patterns of Ag/RGO and Ag/N-RGO

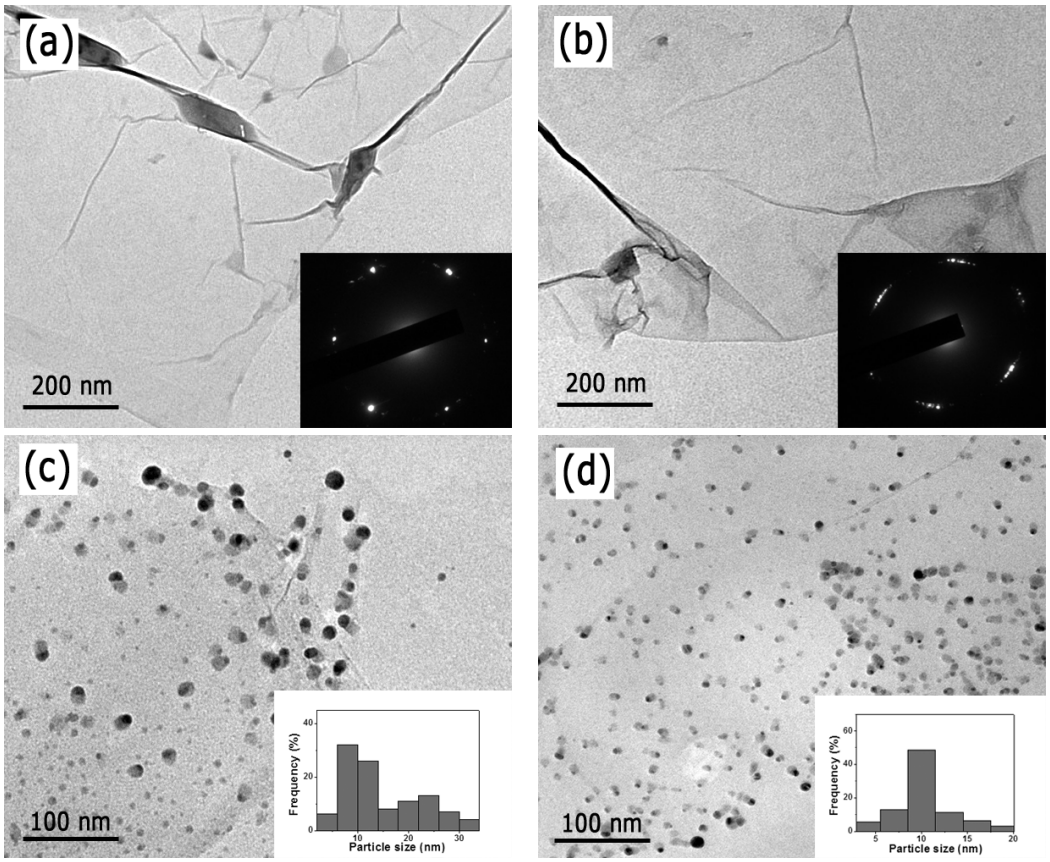

Fig. 2. TEM images of (a) RGO, (b) N-RGO (insets for corresponding SAED patterns), (c) Ag/RGO, and (d) Ag/N-RGO (insets for size distributions of the supported Ag NPs)

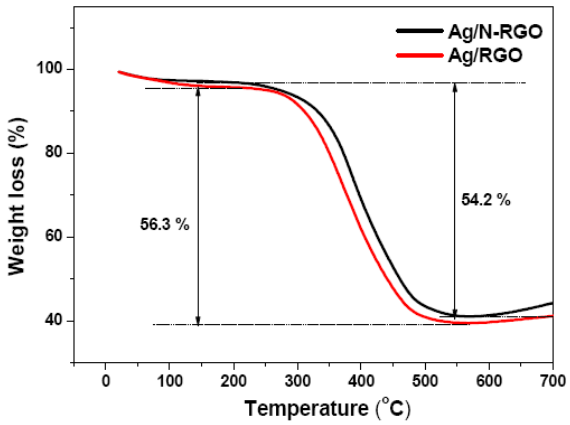

Fig. 3. TGA curves of Ag/RGO and Ag/N-RGO treated under air atmosphere

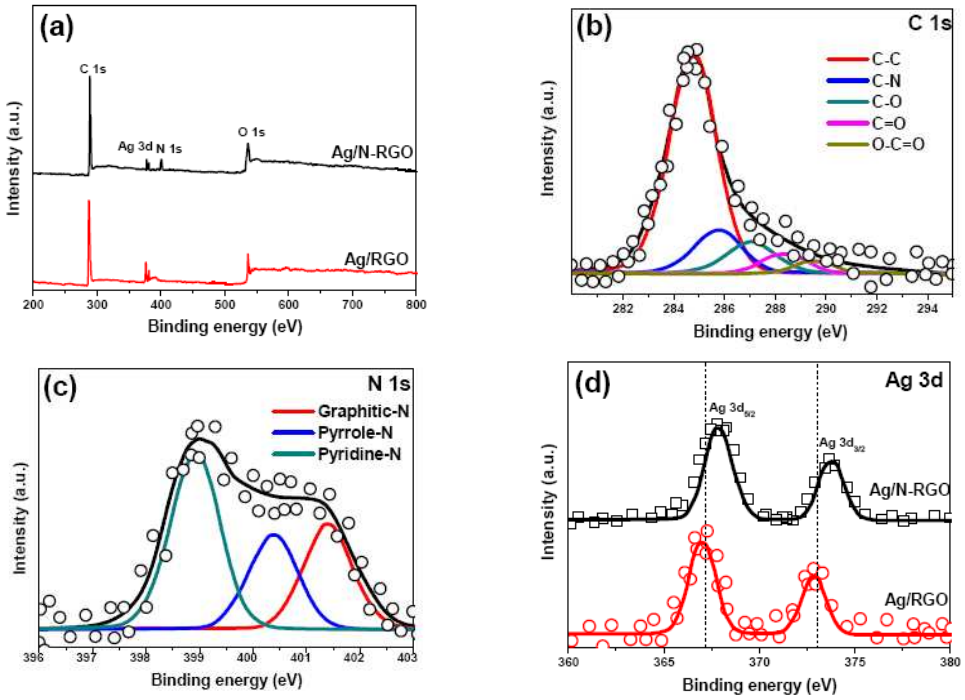

Fig. 4. (a) XPS survey spectra of Ag/RGO and Ag/N-RGO; (b) C 1s, and (c) N 1s spectra of Ag/N-RGO; (d) Ag 3d spectra of Ag/RGO and Ag/N-RGO

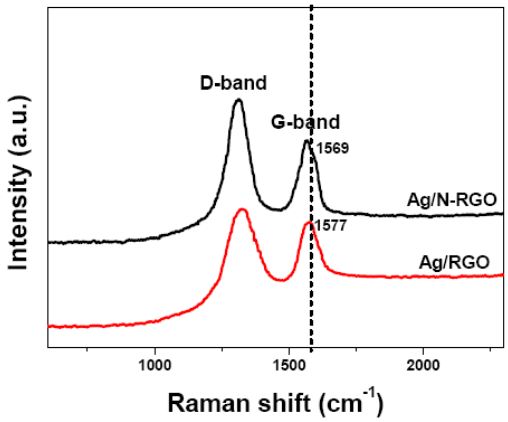

Fig. 5. Raman spectra of Ag/RGO and Ag/N-RGO

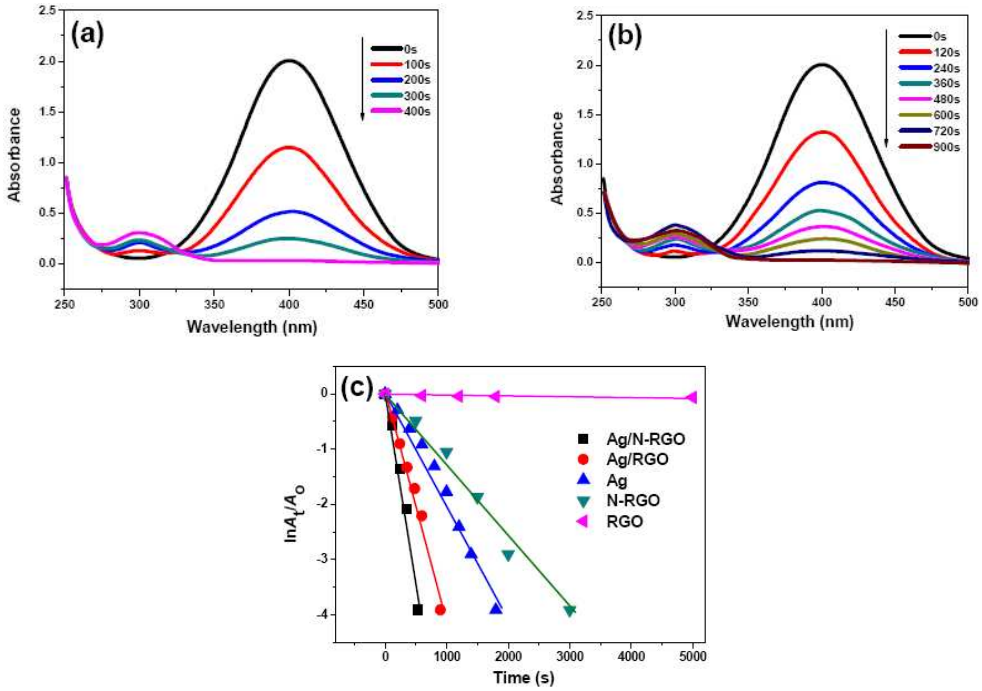

Fig. 6. Time-dependent UV-vis absorption spectra of the reduction of 4-NP by $NaBH_4$ in the presence of (a) Ag/N-RGO and (b) Ag/RGO as catalysts. (c) Plot of A_t/A_0 versus reaction time for the reduction of 4-NP with different catalysts of Ag/N-RGO, Ag/RGO, Ag NPs, N-RGO and RGO.

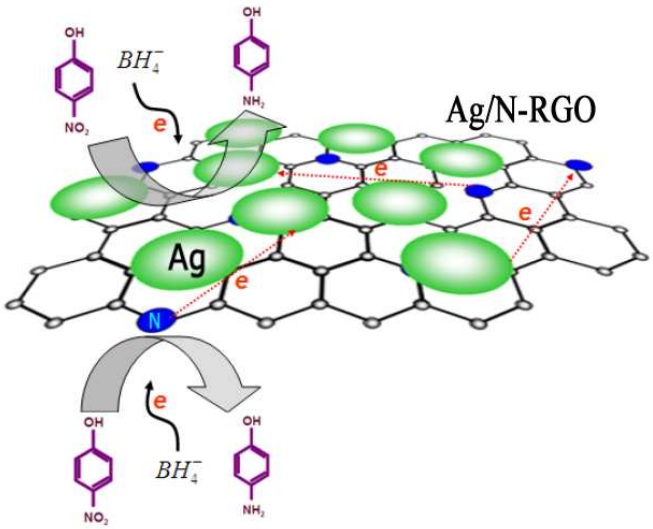

Scheme 2 Possible mechanism for catalytic reduction of 4-NP to 4-NP by $NaBH_4$ with Ag/N-RGO catalyst

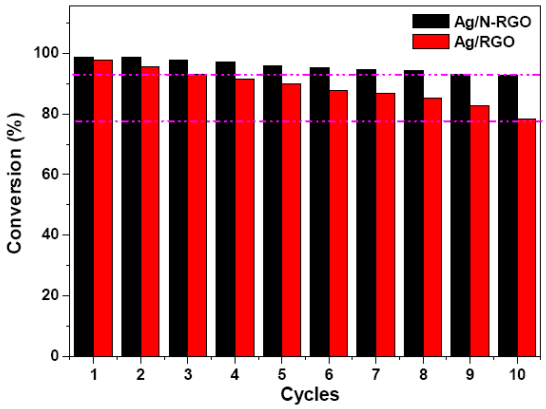

Fig. 7. Conversion efficiency of 4-NP with Ag/RGO and Ag/N-RGO in ten successive cycles

Table 1. Fitting results summary of the XPS spectra of Ag/RGO and Ag/N-RGO

Sample	Element content (at.%)				
	C	O	N	Ag	
Ag/RGO	72.63	15.21	-	12.16	
Ag/N-RGO	69.58	11.67	4.38	14.75	
	C functional groups / (BE, eV)				
	C–C	C–N	C–O	C=O	O–C=O
	284.7	285.8	287.1	288.6	289.7
Ag/RGO	79.64	-	11.86	6.31	2.19
Ag/N-RGO	77.12	9.32	6.75	4.56	2.25
	N functional groups / (BE, eV)				
	Pyridine-N	Pyrrole-N	Graphitic-N		
	398.8	400.3	401.4		
Ag/RGO	-	-	-		
Ag/N-RGO	46.91	21.56	31.53		

Table 2. Summary of the reaction rate constants (k) of the catalysts

Sample	Ag/N-RGO	Ag/RGO	Ag	N-RGO	RGO
k ($\times 10^{-3}$/s)	7.4	3.6	2.1	0.97	0.01